Gait studies for a quadrupedal microrobot reveal contrasting running templates in two frequency regimes

Benjamin Goldberg, Neel Doshi, Kaushik Jayaram and Robert J Wood

Published 15 June 2017

Gait studies for a quadrupedal microrobot reveal contrasting running templates in two frequency regimes

Benjamin Goldberg*[1,2], Neel Doshi[1,2], Kaushik Jayaram[1,2], and Robert J. Wood[1,2]

[1]John A. Paulson School of Engineering and Applied Sciences, Harvard University, Cambridge, MA, USA
[2]Wyss Institute for Biologically Inspired Engineering

Performance metrics such as speed, cost of transport, and stability are the driving factors behind gait selection in legged locomotion. To help understand the effect of gait on the performance and dynamics of small-scale ambulation, we explore four quadrupedal gaits over a wide range of stride frequencies on a $1.43\,\mathrm{g}$, biologically-inspired microrobot, the Harvard Ambulatory MicroRobot (HAMR). Despite its small size, HAMR can precisely control leg frequency, phasing, and trajectory, making it an exceptional platform for gait studies at scales relevant to insect locomotion. The natural frequencies of the body dynamics are used to identify frequency regimes where the choice of gait has varying influence on speed and cost of transport (CoT). To further quantify these effects, two new metrics, *ineffective stance* and *stride correlation*, are leveraged to capture effects of foot slippage and observed footfall patterns on locomotion performance. At stride frequencies near body resonant modes, gait is found to drastically alter speed and CoT. When running well above these stride frequencies we find a gait-agnostic shift towards energy characteristics that support "kinematic running", which is defined as a gait with a Froude number greater than one with energy profiles more similar to walking than running. This kinematic running is rapid (8.5 body lengths per second), efficient (CoT=9.4), different from widely observed SLIP templates of running, and has the potential to simplify design and control for insect-scale runners.

1 Introduction

Nature's elite runners provide rich insight into fast and efficient locomotion, enabling roboticists to push the performance limits of legged robots. In turn, these bioinspired robots can provide the opportunity to test new hypotheses in biomechanics. There are numerous studies on the biomechanics of locomotion, including studies at the centimeter- and millimeter-scale with cockroaches (Full and Tu, 1991), geckos (Chen et al., 2006), and wood ants (Reinhardt et al., 2009). These studies have revealed that mechanics of running animals varying in leg morphology, leg number, and body size can be captured by simple physics-based models called templates (Full and Koditschek, 1999). For example, the spring-loaded inverted pendulum (SLIP) model simplifies the sagittal plane running dynamics into vertical and fore-aft leg forces that act on the body and vary periodically, with vertical leg forces leading fore-aft forces by a quarter period (Blickhan and Full, 1993). Sometimes, however, deviations from this model are observed,

*To whom correspondence should be addressed; E-mail: bgoldberg@g.harvard.edu

as with wood ants described by Reinhardt et al. Furthermore, some of the fastest legged locomotion relative to body size occurs at scales smaller than those previously studied. For example erythracarid mites (body length of $1\,\mathrm{mm}$) can run at speeds up to 192 body lengths per second ($\mathrm{BL\,s^{-1}}$) (Rubin et al., 2016). So far, few explanations for these speeds exist, in no small part due to the challenges in measuring the underlying mechanics at this scale.

Given the nascent phase of designing small scale, bio-inspired robots to approach these remarkable speeds observed in biology, research is typically focused on the manufacturing aspects, for example the flexure-based approaches overviewed in (Haldane et al., 2015), and less on performance characterization . Exemplary flexure-based mobile microrobots that implement new design and manufacturing processes include robots that can walk (Hoover et al., 2008), run (Bailey et al., 2001; Birkmeyer et al., 2009; Haldane and Fearing, 2015), jump (Noh et al., 2012), and climb (Birkmeyer et al., 2012).

Beyond these manufacturing aspects, some studies have explored performance similarities and deviations from findings in animals. For example, SLIP dynamics in palm-sized, legged robots have been reported (e.g., DASH (Birkmeyer et al., 2009)) while others explain deviations from this model (e.g., Sprawlita (Bailey et al., 2001) and VelociRoACH (Haldane and Fearing, 2015)). At similar scales to mites, recent studies have demonstrated the versatility of offboard magnetic actuation to study the effect of gait on speed and body oscillations while traversing rough terrain with sub-2g robots (St Pierre and Bergbreiter, 2016; Vogtmann et al., 2017).

One of the smallest, fastest, and highly articulated legged robots is the Harvard Ambulatory MicroRobot, HAMR (Fig. 1a). HAMR is an insect-scale quadrupedal robot fabricated using mesoscale, PC-MEMS manufacturing techniques (Sreetharan et al., 2012) and is a multipurpose legged platform. It has been shown to run at speeds above $10\,\mathrm{BL\,s^{-1}}$ ($44\,\mathrm{cm\,s^{-1}}$) (Baisch et al., 2014), climb inclines of 22° (Seitz et al., 2014), and perform autonomous heading control (Bruhwiler et al., 2015).

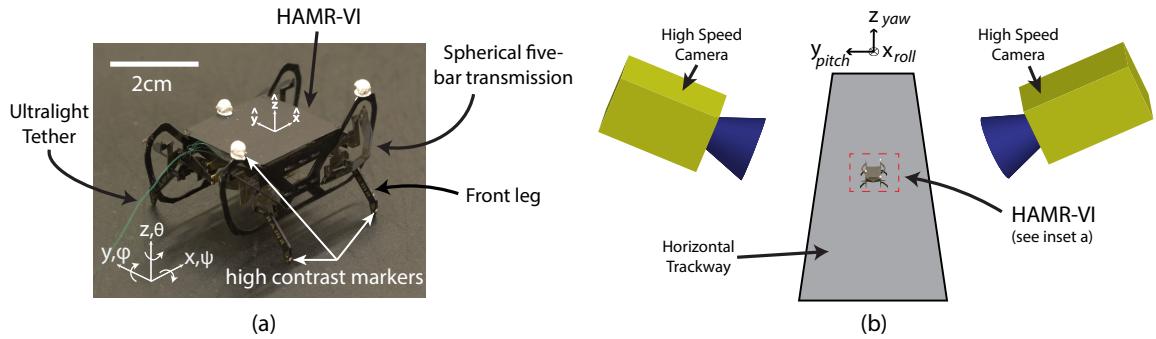

Figure 1: (a) The Harvard Ambulatory MicroRobot (HAMR-VI) with the body and feet tracking markers. (b) Locomotion trackway for motion capture of HAMR described in (Goldberg et al., 2017a). Two high speed cameras perform a stereo, 3D-reconstruction for the body and four feet.

Compared to most other legged systems, the piezoelectric actuators that drive the flexure-based leg transmissions in HAMR allow for unnaturally high stride frequencies. The highest speeds with HAMR are achieved using stride frequencies that are more than twice those typically seen at the same scale in biology – well above the body natural frequencies. Most robotic runners have similar stride frequency limitations, imposed by either the robot morphology or actuator bandwidth. Similarly, animals have a bandwidth limit on their muscles after which speed becomes nearly independent of stride frequency, and further increases in speed are attributed to changes in gait and stride length (Holmes et al., 2006).

While a similar approach for HAMR could be taken, we wish to leverage the high bandwidth of the piezoelectric bending bimorph actuators to operate beyond body resonance. This is similar in spirit to (Haldane et al., 2013) where high bandwidth electromagnetic motors are use to achieve stride frequencies

higher than the body dynamics. In contrast to rotary motors where peak torque is produced at stall, piezoelectric actuators have force generation that is independent of actuation frequency up to actuator resonance (Jafferis et al., 2016a). We wish to leverage this property and operate in frequency regimes suited for different tasks; for example, precision quasi-static motions for orienting a vision system, using body resonance to negotiate over obstacles, or exploiting transmission resonance for high speed running. The high bandwidth and power characteristics of piezoelectric actuators allow the potential for all of these tasks and this paper addresses the effects of gait selection on performance in low and high frequency regimes.

In this paper, we describe the control capabilities of HAMR and the methods and metrics used to analyze its locomotion (Sec. 2). In Section 3, we describe the results of the experimental gait studies. We find that there are distinct differences in body kinematics and dynamics in low and high stride frequency regimes (Sec. 3.1) that result in variations in locomotion performance (e.g., speed and cost of transport (CoT)). At stride frequencies from 50-65Hz, speed is similar across substantial variations in gait (Sec. 3.2). In Sec. 3.3, we discuss the energy and force characteristics of HAMR and show that it follows a reduced order SLIP model in the body dynamics regime but deviates from this model at high frequencies (Sec. 3.3). In this regime where stride frequencies surpass the body resonant modes, we observe "kinematic running" profiles, high speeds, high average step displacement, and low CoT across wide variations in gait and without any changes in body morphology. We define "kinematic running" as locomotion with a Froude number greater than one with horizontal kinetic energy and potential energy that is more similar to a walking template rather than a running template. In Section 3.4, we discuss challenges with achieving high speeds and low CoT by leveraging new metrics of footfall correlation and ineffective stance. A cross-platform analysis (Sec. 3.5) shows that "kinematic running" gaits with HAMR have comparable speeds and CoT compared to other runners at this scale, with speeds upwards of 8.5 BL/s, and CoTs lower than 9.4. Finally, we conclude with an outlook on the implications of running at small scales (Sec. 4) and future work (Sec. 5).

2 Methods

2.1 Platform Overview

HAMR is a 1.43g quadrupedal microrobot with eight degrees of freedom (DOFs) – one lift and one swing DOF per leg (Fig. 2a). The quadrupedal morphology was chosen to reduce manufacturing complexity and overall size compared to earlier hexapedal HAMR prototypes (Baisch and Wood, 2011), while enabling both quasi-static and dynamic operation. This design choice was further motivated by rapidly running cockroaches, which sometimes use quadrupedal or bipedal gaits at high speeds (Full et al., 1991).

The PC-MEMS fabrication process allows for fast and repeatable assembly of HAMR's complex spherical five-bar (SFB) leg transmissions despite its small scale (Baisch et al., 2014). Each DOF is driven by a piezoelectric actuator which allows HAMR to run at stride frequencies exceeding $100\,\mathrm{Hz}$. Baisch et al. measured speeds on a previous version of HAMR (HAMR-VP) for the trot gait, observing a top speed of $44\,\mathrm{cm\,s^{-1}}$. In these studies, HAMR was limited to three standard quadrupedal gaits due to the mechanical coupling between contralateral swing DOFs. The three allowable gaits were the walk, trot, and pace (only the trot, however, was implemented).

Recent design modifications to the powertrain and the addition of two actuators has resulted in two independently-actuated DOFs for each leg. These modifications give HAMR-VI a 114% increase in the payload carrying capacity, larger step displacements, and the potential to achieve aerial phases (Doshi et al., 2015). In addition, with eight independently actuated DOFs, HAMR can now achieve any arbitrary gait including standard quadrupedal gaits such as the jump, bound, and pronk. Example actuator signals for a single leg during a $50\,\mathrm{Hz}$ pronk gait are shown in Fig. 2b with the leg trajectories shown in a

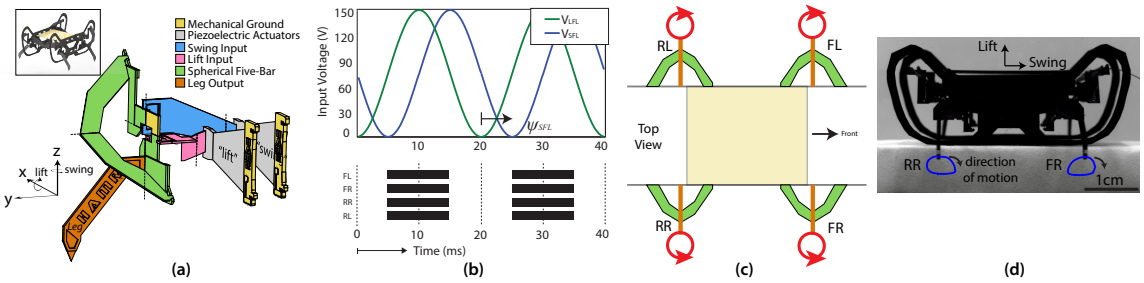

Figure 2: a) Perspective view of the 2-DOF, single-leg, spherical five-bar (SFB) transmission with lift and swing DOFs labeled. b) Example open-loop actuator input signals for a 50 Hz stride frequency and corresponding footfall patterns for the pronk gait with black bars indicating stance phase. c) Top view of whole robot with leg naming convention and theoretical leg trajectories in red. d) Side view of HAMR on blocks with tracked 50 Hz leg trajectories in air for the front right ("FR") and rear right ("RR") legs.

schematic of a top view projection (Fig. 2c) and tracked video frames of the robot suspended in air (Fig. 2d). The footfall patterns for the trot (previously implemented) and three newly implemented gaits on HAMR – the pronk, jump, and bound – are shown in Fig. 3. The ability to control each of the eight DOFs of HAMR independently opens up a very large parameter space for gait control. The control inputs for the actuators are outlined and described in the following section. All tests in this paper are for level-ground, straight-line, steady-state locomotion.

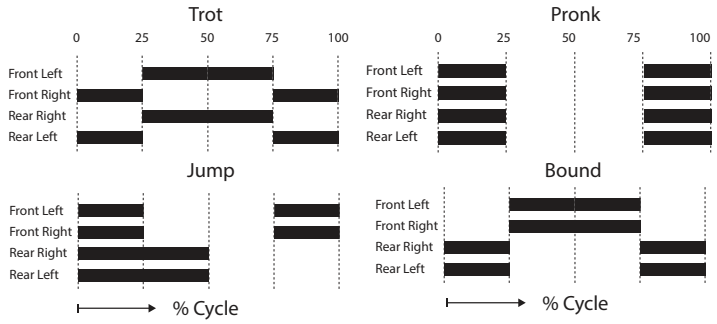

Figure 3: Open-loop commanded footfall patterns for four standard quadrupedal gaits tested in this paper. Black bars indicate planned ground contact.

2.2 Control Inputs

Understanding the effect of control inputs on performance is critical to establish in order to guide future optimization studies of small scale running robots. This study focuses on the effect of three control inputs for HAMR, variations that are also commonly observed in biology: stride frequency, input energy, and leg phasing. These control inputs are tested given the HAMR-VI body morphology and are described below. Rapid testing of these control inputs is enabled by a 10-wire power and control tether and considerations for how these results apply to a power autonomous robot are discussed in Sec. 3.5.

2.2.1 Frequency

The stride frequency is tested from 10-65Hz. This range encompasses the body dynamics regime (described in Sec. 3.1), and approaches the resonance of the SFB transmission. Although the actuators can

be driven at frequencies exceeding $65\,\mathrm{Hz}$, transmission resonance is around $70\,\mathrm{Hz}$ which impairs smooth locomotion. A complete frequency analysis of the actuators and the SFB is explored in (Doshi et al., 2017).

2.2.2 Input Energy

The actuator bias voltage, V_{bias}, is tested from 90-150V, which is directly related to the input energy per stride ($E \propto V_{\text{bias}}^2$). These voltages correspond to an input energy ranging from 0.65-1.8$^{\mathrm{mJ}}/_{\mathrm{stride}}$ and this relationship is described further in Supplementary Material, S5. The input energy for each trial is manually tuned to achieve the fastest run, consistent with (Baisch et al., 2014)[i]. We assume that the lift voltage controls the force in the vertical DOF (z) and the swing voltage controls force in the fore/aft DOF (x) before resonance of the SFB transmission. The effect of input energy on CoT for all of the gaits is discussed in Sec. 3.3.

2.2.3 Phasing

As described in Sec. 2.1, HAMR-VI can achieve any arbitrary gait. For actuator phasing, there are two subsets of leg phase variations: *inter-leg* and *intra-leg* phasing. While both directly affect gait, there are distinct differences between the two. Inter-leg phasing controls the variation in footfall timing between each of the individual legs whereas intra-leg phasing controls the direction and duration of leg footfalls (i.e., the foot trajectory). In this work, inter-leg phasing is used to command standard quadrupedal gaits. The four gaits tested in this paper are the trot, pronk, jump, and bound. Gait phasing is commanded to the actuators in an open-loop sense, however, and can differ from the observed footfall timings. To quantify these deviations, a correlation analysis is described in Sec. 2.3 to determine how closely the footfall matches the commanded gait. Intra-leg phasing is reserved for turning maneuvers and is explored in (Goldberg et al., 2017b).

2.2.4 Selection of the trials

A total of 64 trials are conducted, spanning the four different inter-leg gait phasings and eight different stride frequencies (10, 15, 20, 25, 50, 55, 60, 65 Hz), with each gait tested twice at each condition. The trials are selected based on the frequency analysis for the body and leg dynamics described in Sec. 3.1.3. The tests are randomized to minimize the temporal degradation effects of the robot (e.g changes in flexure stiffness, foot coefficient of friction, etc.) on the performance metrics, and each trial captures only steady-state behavior[ii].

2.3 Locomotion Metrics

Conventional locomotion metrics such as speed, average step displacement, CoT, relative stiffness, Froude number, duty factor, and pendulum-like energy recovery are measured for each of the 64 trials. Based on these metrics, we define "high performance" locomotion as being a combination of two or more of the following: high speed, high average step displacement, and low CoT. For HAMR-VI, we define these thresholds as greater than $6\,\mathrm{BL\,s^{-1}}$ (Froude number greater than 0.75), greater than $4.7\,\mathrm{mm\,stride^{-1}}$ (quasi-static step length), and a CoT lower than 20 (similar to biological runners at this scale – e.g. from Full et al., 1990).

[i] Leg phase, however, is not tuned (as is done in Baisch et al.) so that open-loop gait commands are preserved.

[ii] The settling time for the first cycle to be within $\pm 10\%$ mean velocity in gaits that successfully reach steady-state is experimentally measured to be approximately $T_s = 0.3\,\mathrm{s}$ across all stride frequencies.

To help further quantify the underlying mechanics of locomotion, two new metrics, *ineffective stance* and *footfall correlation*, are defined in the following sections. The aim for these metrics is to compare and contrast gaits and frequency regimes where body dynamics and foot slippage significantly affect locomotion. A complete MATLAB structure for all operating conditions and metrics is provided in Supplementary Material, S7.

2.3.1 New metric definitions

Ineffective stance Foot slippage is often observed in animals and robots during locomotion involving perturbations or on complex terrains (Jusufi et al., 2008; Mazouchova et al., 2010; Roberts and Koditschek, 2016). A normalized metric for foot slippage, however, has not yet been established. Prior studies looking at foot slippage have used metrics such as *stride success ratio* (Jayaram and Full, 2016) and *step displacement* (Mazouchova et al., 2013). These metrics work well when the amount of foot slippage is binary (foot does or does not slip) or aggregated over all of the legs. However, these measures do not quantify slippage as a portion of the stride or capture variations between individual legs.

A new metric, ineffective stance ($\mathrm{I_s}$), quantifies the percentage of the gait cycle that is neither "swing" nor "stance". The gait cycle is considered to consist of three categories: swing, stance, and ineffective stance. In an ideal gait cycle, the amount of time for swing and stance can be described as the following:

> ***Swing***: Amount of time the foot is above the ground ($p_{wz,i} > 0$) *and* is swinging forward in a body-fixed frame ($v_{bx,i} > 0$).
>
> ***Stance***: Amount of time the foot is planted on the ground ($p_{wz,i} = 0$) *and* has zero velocity relative to a fixed world frame ($v_{wx,i} = 0$).
>
> ***Ineffective Stance***: Amount of time that the leg is slipping on the ground ($p_{wz,i} = 0 \,\&\, v_{wx,i} < 0$) *or* swinging backwards in air ($p_{wz,i} > 0 \,\&\, v_{bx,i} < 0$).

where p and v are the foot positions and velocities in the body (b) or world (w) frames for the x- and z-DOFs of i^{th} foot. Quantitatively, these categories make up the total time, T_{total}, of the cycle(s) of the gait being analyzed:

$$T_{\text{total}} = T_{\text{swing}} + T_{\text{stance}} + T_{\text{ineffective-stance}} \tag{1}$$

As a percentage, ineffective stance is defined as $\mathrm{I_s} = {}^{T_{\text{ineffective-stance}}}/_{T_{\text{total}}}$. Ineffective stance is measured for each of the legs but can be averaged to get a single measure of ineffective stance for the whole system, $\bar{\mathrm{I}}_\mathrm{s}$. Qualitatively, ineffective stance is depicted in Fig. 4a. The automated foot tracking algorithm described in (Goldberg et al., 2017a) is used to reconstruct the 3D position of all four feet, and thus, measure ineffective stance.

We hypothesize that non-zero levels of ineffective stance are to be expected as HAMR has not been tuned to run at a particular operating condition and does not utilize feedback control to overcome natural variations (e.g. manufacturing, surface, stiffness, etc.). Furthermore, foot design typically has a large effect on ineffective stance and a comparative study of foot/adhesion designs is subject of future work. This will leverage these metrics and measured performances as a baseline for results and methodology.

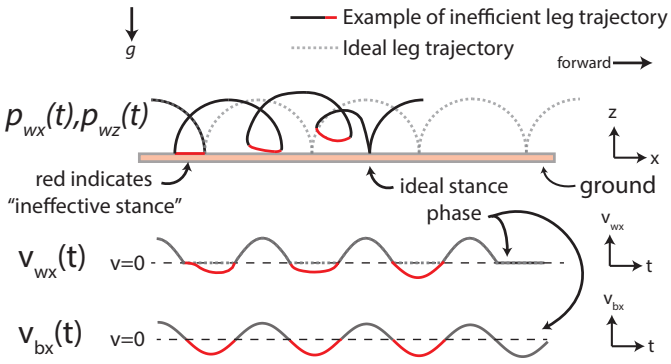

Figure 4: This schematic shows an example of a foot trajectory in the sagittal plane as a function of time, t, with non-zero levels of ineffective stance. The top traces are drawn in a world reference frame as a projection onto the x-z plane. The velocities (middle and bottom traces) are considered both the world and body frames.

Footfall correlation with gait commands Another foot metric that is used in this study is the correlation coefficient for each foot, ρ_i, of the mean-subtracted footfall pattern, X_i, with the mean-subtracted drive signal, Y_i:

$$\rho_i = \frac{X_i \cdot Y_i}{||X_i|| ||Y_i||} \tag{2}$$

The correlation coefficient is computed for the foot z-displacement as a function of time ($X_i = p_{wz,i}(t)$) and the commanded voltage ($Y_i = V_i(t)$) for each individual lift-DOF. The z-DOF is used to give a measure of correlation with the footfall pattern – i.e. how well the kinematics follow the drive signal. The correlation coefficient, ρ, is an average between all four legs.

The same method is applied to measuring correlation with horizontal and gravitational potential energy in Sec. 3.3.1, where X_i is the theoretical SLIP energy profile (i.e. horizontal kinetic or gravitational potential energy) and Y_i is the measured energy profile.

Amplitude-normalized stride correlation A new metric called amplitude-normalized stride correlation (ANSC) was introduced in Goldberg et al. (2017a). ANSC is a dimensionless quantity that measures the periodicity and amplitude of body oscillations during running. While the implications of the relative quantities of ANSC are yet to be determined, baseline quantities for HAMR gaits and three other legged systems are reported in Supplementary Material, S6.

2.4 Experimental Setup: Recording Kinematics

A schematic of the locomotion trackway and motion capture arena is shown in Fig. 1b. A description of the motion capture methodology and an accuracy analysis is described in (Goldberg et al., 2017a). There are two high speed cameras (Vision Research, Phantom v7.3) mounted on either side of the robot sagittal plane. The frame rate (fps) for the cameras is set to 30 times the stride frequency. At the highest tested stride frequency of 65 Hz, this corresponds to 1950 fps. Only trials that result in straight locomotion and reach steady state are used for analysis. Robot dimensions are shown in Table 1a.

The 3D foot positions are reconstructed using a '1.5 camera' reconstruction method described in Goldberg et al. (2017a). The running surface is black cardstock adhered to the aluminum trackway with spray adhesive (3M, Super77). Signal generation is run at 5 kHz (MathWorks, Simulink Real-Time).

2.5 Robot baseline parameters and performance

To establish the robot as a platform capable of testing biological hypotheses, the performance needs to be repeatable. To ensure that the robot has similar performance for multiple trials with the same operating conditions, four identical trials (each with at least six cycles) are run at three test frequencies of 10 Hz, 25 Hz, and 60 Hz. A summary of the these results are shown in Table 1b. Even when strongly influenced by body dynamics at 25 Hz, the speeds are still within 7% of each other for a given robot and operating condition.

Table 1: (a) HAMR morphology and (b) Repeatability of speed for three trot gaits. Speeds represents mean speed $\pm$ 1 s.d for four separate trials at each drive condition with six steps. Speeds between trials of the same gait are within 7% of each other.

Parameter	Value
Body Dimensions ($l \times w \times h$)	$4.51 \times 3.45 \times 2.30$cm
Hip Height	0.98 cm
Mass	1.43 g

(a)

Trot Conditions	Speed (cm/s)
10 Hz at $^{1.8\,\mathrm{mJ}}/_{\mathrm{stride}}$ (n=4)	8.0 ± 0.46
25 Hz at $^{0.65\,\mathrm{mJ}}/_{\mathrm{stride}}$ (n=4)	8.6 ± 0.56
60 Hz at $^{0.65\,\mathrm{mJ}}/_{\mathrm{stride}}$ (n=4)	37.7 ± 2.0

(b)

2.6 Statistics

Statistical analysis is performed using a repeated measures ANOVA in MATLAB (MathWorks, 2015b). Sixteen unique drive conditions (four stride frequencies, four gaits, and one input energy) are tested in each of the frequency regimes (low and high). Each drive condition is tested twice for a total of 64 trials (32 in each regime). The response was the performance metric (average step displacement, CoT, correlation, etc.), and we report the P value and F ratio in APA format to support/reject our hypothesis. Significance is tested at a level of $\alpha = 0.05$.

3 Results

The analysis is divided into the following five sections where we describe the main conclusions of the gaits studies:

1. Frequency-dependent behavior for HAMR is grouped into two regimes.
2. High performance is attainable in low and high frequency regimes.
3. "Kinematic running" is observed in the high frequency regime which leads to high performance and simplified control.
4. The main challenge for achieving high performance is with ground contact affecting prescribed footfall patterns (i.e. high ineffective stance and low footfall correlation).
5. The net performance of HAMR is similar to other legged systems at its scale.

3.1 Frequency-dependent behavior

3.1.1 Theoretical body mode resonance

The theoretical body resonance for the z mode is assumed to follow the SLIP model, with the stiffness, k, being the combined linear spring stiffness of four parallel powertrains. The resonant frequency, f_n, is then: $f_n = (1/2\pi)\sqrt{k/m}$ where m is the mass of the robot. The combined powertrain stiffness can be determined by measuring the sag height in response to incrementally adding weights to the back of the robot. The stiffness is shown to be approximately linear with displacement in (Baisch, 2013), and for

HAMR-VI, the stiffness is $24\,\mathrm{N\,m^{-1}}$ which corresponds to a resonant frequency of $20\,\mathrm{Hz}$. Due to the inherent nonlinearities of the system (e.g. ground contact and the SFB transmission) and gaits with more than one instance of ground contact per cycle (all except pronk), the body resonance can be excited with stride frequencies below $20\,\mathrm{Hz}$. During the trot, for example, alternating footfalls result in an effective excitation frequency of $20\,\mathrm{Hz}$ for a $10\,\mathrm{Hz}$ stride frequency. An experimental characterization of the resonant modes is conducted in the following section.

3.1.2 Experimental resonance

The body modes of the robot are experimentally identified by sending a linear chirp signal to excite a single body mode of the robot. For example, the z mode is excited by actuating only the lift actuators in phase with each other and holding the swing leg DOF fixed in a slotted acrylic fixture. The body natural frequency is identified by computing the FFT of the robot height. The *roll* body mode is actuated with ipsilateral lift DOFs in phase and contralateral lift DOFs out of phase. The opposite is commanded for the *pitch* mode with contralateral lift DOFs in phase and ipsilateral lift DOFs out of phase. These drive schemes are indicated in the circular foot markings of the schematics in Fig. 5.

The resonant peaks occur at 14Hz, 32Hz, and 23Hz for the z, *roll*, and *pitch* modes respectively as shown in the linear frequency sweeps in Fig. 5. Compared with the resonant frequency of $20\,\mathrm{Hz}$ in the previous section for the z mode, the experimental resonance of $14\,\mathrm{Hz}$ is 30% lower than predicted. This deviation could be due to variable footfall contacts and changes in apparent stiffness with the applied force of the actuators. These experimental conditions, however, are consistent with the tested gaits and therefore these resonances are assumed to be representative of the true body modes. The three DOFs not considered here (x, y, and *yaw*) are assumed to have a resonance similar to the z, *roll*, and *pitch*

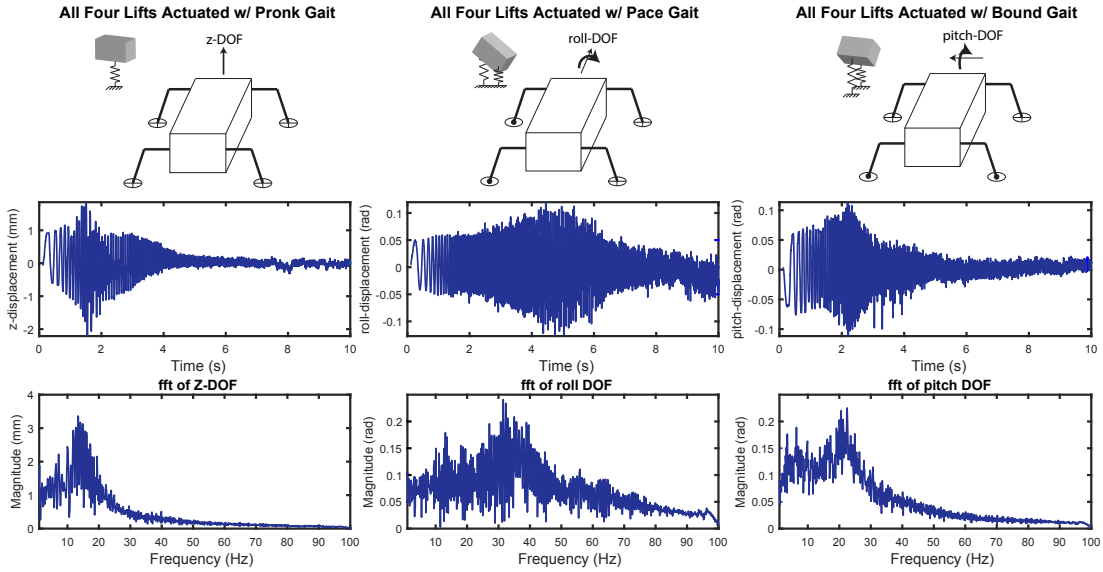

Figure 5: Ten second linear frequency chirps (0-100Hz) are commanded with three different inter-leg phasings to experimentally determine the body natural frequency for the z, *roll*, and *pitch* modes. These chirp signals are sent to the lift actuators while holding the swing DOF fixed. An 'X' on the foot indicates pushing on the ground and a '·' indicates lifting off the ground. The displacements in the time-domain are shown in the second row and the FFTs are shown in the third row. The resonant peaks occur at 14Hz, 32Hz, and 22Hz for the z, *roll*, and *pitch* modes respectively.

(14-32Hz) since the stiffnesses and inertias have similar values as the tested DOFs (Doshi et al., 2015).

Blickhan and Full show that in organisms, running animals over a wide range of sizes and running speeds have a normalized relative stiffness of approximately 10 (Blickhan and Full, 1993). This indicates that the relative individual leg force is roughly ten times greater than the relative compression of the whole-body leg spring, regardless of animal size and running speeds. Based on the body mode analysis above, HAMR has a relative stiffness of 4.3 assuming a pronking gait, slightly lower than the trends seen in other legged systems. Relative stiffness, however, can be modulated by altering the input energy, and implications of this are discussed in Sec. 3.3.

3.1.3 Selection of two frequency regimes

Two distinct frequency regimes are identified to describe the locomotion characteristics of HAMR. One, the low frequency, or "body mode" regime, is considered to be from 10-25Hz. Based on the analysis in 3.1, this is the regime that is most influenced by sagittal plane oscillations (z and *pitch*). The second regime, the high frequency regime, is from 50-65Hz. This regime is selected because the analysis in Sec. 3.1 shows that sagittal plane oscillations are attenuated above $50\,\mathrm{Hz}$.

Prior work with HAMR indicates similar average step displacements in the medium frequency regime (30-45Hz) compared with the high frequency regime before transmission resonance (Baisch et al., 2014; Goldberg et al., 2017a). Therefore, the 30-45Hz stride frequency regime is not tested in order to focus on the regime where highest speed locomotion is achieved, and to highlight the differences between the body dynamics regime and high speed, high stride frequency regime. Therefore, the 64 trials described in Sec. 2.2 are grouped into two categories: low and high frequency, with 32 trials in each category.

3.2 Speed and average step displacement characterization

The following sections describe the performance of the gaits in the context of the two regimes: low frequency (10-25Hz) and high frequency (50-65Hz).

Forward velocities ($\overline{u}$) ranged from $-6.1\,\mathrm{cm\,s^{-1}}$ to $44.5\,\mathrm{cm\,s^{-1}}$. Velocity varied with gait, stride frequency (f), and input energy. Figure 6a shows the results of each stride of the 64 trials. An example

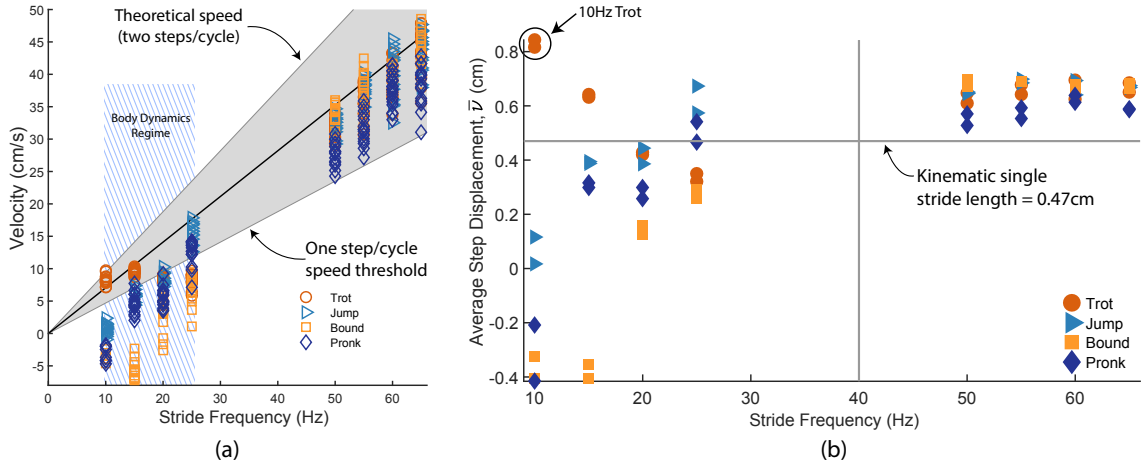

Figure 6: (a) Robot velocity for each stride of the 64 trials. The robot is slower than the predicted kinematic speed (velocity given a $0.47\,\mathrm{cm}$ step length at $1.8^{\mathrm{mJ}}/_{\mathrm{stride}}$) in the body dynamics regime but closer to this threshold in the high frequency regime. (b) Average step displacement vs. frequency. The horizontal line indicates the nominal stride length for HAMR of $0.47\,\mathrm{cm}$ at $1.8^{\mathrm{mJ}}/_{\mathrm{stride}}$.

of a tracked trial, the $10\,\mathrm{Hz}$ trot, is shown in shown electronic supplementary material, video S1, and a qualitative comparison of the four tested gait types at a $60\,\mathrm{Hz}$ stride frequency is shown in electronic supplementary material, video S2.

The average step displacement, $\overline{\nu} = \overline{u}/f$, is used to compare relative performance of gaits with varying stride frequencies. One of the gaits that has the highest average step displacement, the $10\,\mathrm{Hz}$ trot, is in the low frequency regime. It is hypothesized that this is due to constructive influence of body dynamics on performance. However, some of the lowest performing gaits are also in this regime. With these gaits, the direction of travel is unintentionally reversed, most likely due to destructive interference of body dynamics. These observations indicate that gaits in the low frequency regime have high variation in average step displacement ($0.26 \pm 0.35\,\mathrm{cm\,step^{-1}}$, n=32) due to the influence of body resonant modes. In contrast, gaits in the high frequency regime show much lower variation in average step displacement ($0.65 \pm 0.04\,\mathrm{cm\,step^{-1}}$, n=32), despite the same variations in gait as the low stride frequency regime. Comparing the two regimes, there is a significant difference in average step displacement [ANOVA, $P < 0.001, F_{(3,42)} = 12.7$; Fig. 6b]. Video S3 in the electronic supplementary material shows the progression of the pronking gait with increasing stride frequency with low (and/or negative) average step displacement in the body dynamics regime and high average step displacement in the high frequency regime.

3.3 Energy considerations and "kinematic running"

In this section, we describe the energy characteristics of the locomotion patterns of HAMR within the context of the SLIP running model and CoT.

3.3.1 SLIP Dynamics

Running in animals (independent of body size, morphology, and number of legs) is typically characterized by the SLIP running template where the horizontal kinetic energy (HKE) and gravitational potential energy (GPE) are in-phase. Additionally, this model has typical ground reaction force patterns where the vertical force (F_z) leads the horizontal force (F_x) by 90 degrees (Blickhan and Full, 1993). In contrast, walking dynamics are characterized by the HKE and GPE being nearly 180 degrees out of phase (Cavagna et al., 1977). Correlation with these locomotion templates is measured by computing an average correlation coefficient between the template and experimental GPE, HKE, F_z, and F_x.

The running dynamics of HAMR are analyzed by plotting force and energy traces as a function of time[i]. An example of one of the best per-stride gaits (high average step displacement) is the trot at $10\,\mathrm{Hz}$. Representative force and energy traces for this trial are shown in Fig. 7a. These patterns closely follow SLIP dynamics with the HKE and GPE being in-phase and F_z leading F_x by approximately 90 degrees. The correlation with SLIP energy profiles is 0.86. Another gait that closely matches the SLIP profiles is the $15\,\mathrm{Hz}$ trot (Fig. 7b) with a SLIP energy correlation of 0.72. These two gaits have relatively low energy recovery (2.2% and 3.3%, respectively), as is typical of running animals (Cavagna et al., 1977). Asymmetries in the support phase of the trot gaits in Fig. 7 are due to a lack of a tripod of support with the quadrupedal morphology that causes asymmetric half-strides.

Other gaits (e.g. pronk, jump) with HAMR around this stride frequency, however, do not exhibit energy profiles that match conventional walking or running templates. These observations are likely due to footfalls that are not well matched with the body dynamics which ultimately leads to lower speeds. However, video S4 in the electronic supplementary material shows that highly dynamic, open-loop gaits such as bipedal running and pronking are possible in the body dynamics regime by finely tuning and exploiting the open-loop instabilities of HAMR. Unfortunately, these gaits are highly sensitive to input

[i]The forces are obtained by differentiating the body COM positions.

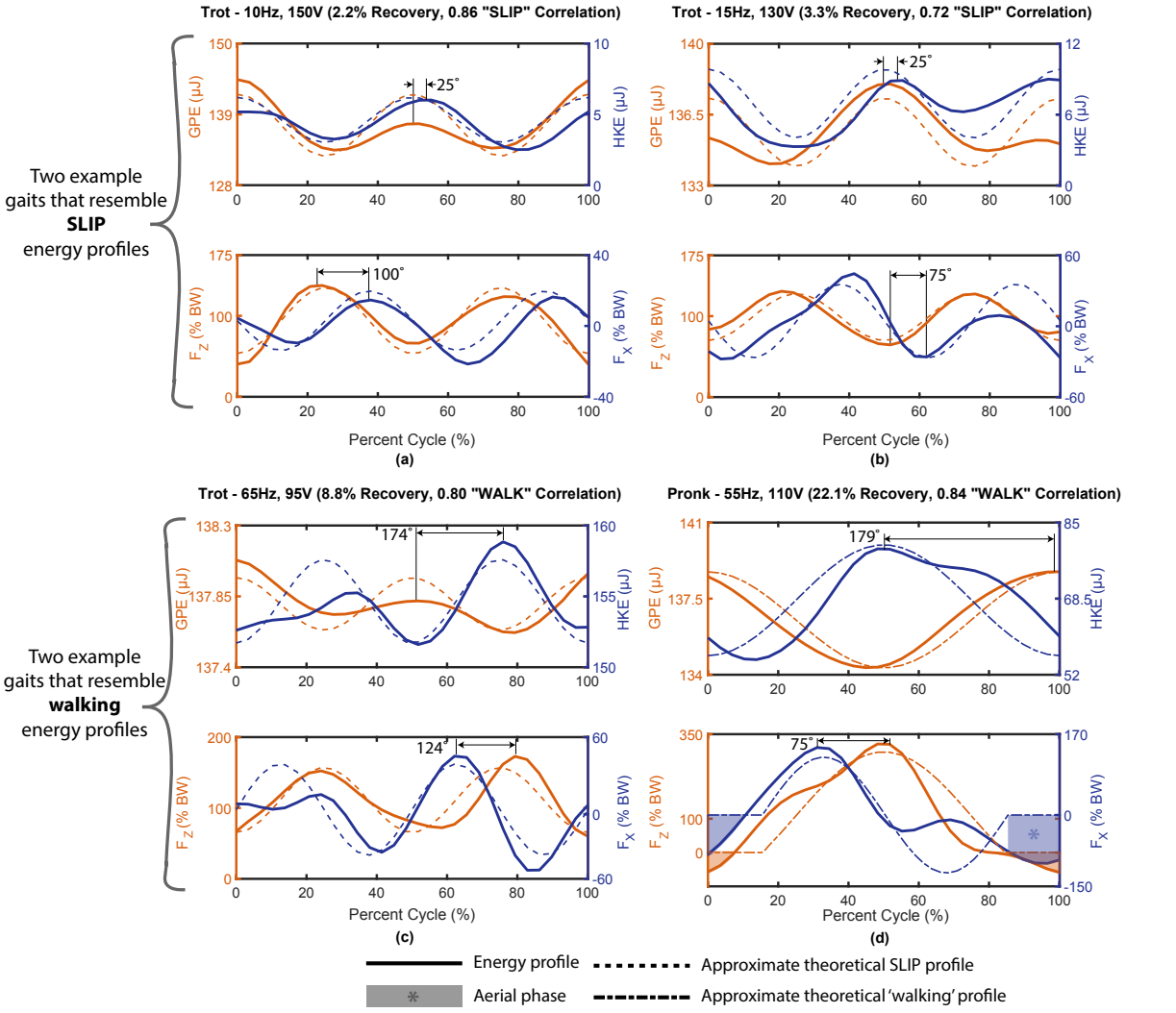

Figure 7: Energy and force traces for the **(a)** 10 Hz trot (n=2 cycles, Fr= 0.07), **(b)** 15 Hz trot (n=4 cycles, Fr= 0.10), **(c)** 65 Hz trot (n=3 cycles, Fr= 2.0), and **(d)** 55 Hz pronk (n=2 cycles, Fr= 1.0). The GPE and HKE for the SLIP profiles are approximately in-phase in contrast to the gaits that match energy profiles of walking (out of phase). Whole body forces for the SLIP profiles have the z-force leading the x-force by approximately 90°. For gaits that match walking profiles, the x-force leads the z-force by approximately 90°. Percent recovery for gaits that match walking profiles have a higher pendulum-like energy recovery compared to gaits that match SLIP profiles (8.8% and 22.1% vs. 2.2% and 3.3%). For the 55 Hz Pronk, there is an aerial phase for approximately 20% of the cycle.

variations and in order to make them repeatable, feedback control or design modifications are necessary for stabilization.

In contrast to the two SLIP-like gaits, two examples of high frequency gaits are shown in Fig. 7c and d. These gaits have energy profiles that are more similar to pendulum-like walking rather than SLIP-like running. The correlation with pendulum-like energy profiles is 0.80 and 0.84 for the 65 Hz Trot and 55 Hz Pronk, respectively. Most gaits in the high frequency regime exhibit this type of kinematic running behavior where HKE and GPE are nearly out of phase, despite Froude numbers greater than one. Looking more closely at the energy characteristics, the two high frequency gaits show higher energy recovery (8.8% and 22.1%) compared to 2.2% for the SLIP-like, 10 Hz trot in low frequency regime. This higher percent recovery is an indication of walking dynamics (Heglund et al., 1982; Bailey et al., 2001). Table 2 summarizes the speeds achieved with the gaits shown in Fig. 7.

3.3.2 Cost of Transport

Cost of transport is a benchmark measurement of the energy efficiency of a mobile system and is defined as the power cost of moving a unit mass of the system a unit distance. The cost of transport reported in this paper is a dimensionless measure of the metabolic cost of transport, CoT $= P/mg\bar{u}$. Here, P is the average input electrical (or metabolic) power, m is the mass, g is the acceleration due to gravity, and $\bar{u}$ is the average velocity (all in SI units). Cost of transport can be measured on HAMR by measuring the input electrical power to the piezoelectric actuators. An estimate of the power for HAMR is described in Supplementary Material, S5.

In this paper, voltage was used as a way to tune the input energy. Since the actuators are primarily capacitive in nature, changing the input electrical energy corresponds to a proportional change in mechanical energy to the system. Using this input variation, HAMR has the ability to achieve higher forces and therefore higher foot displacements and velocities given a constant stride frequency. Since we tuned the input energy to achieve the fastest run for all trials, more efficient locomotion is possible by minimiz-

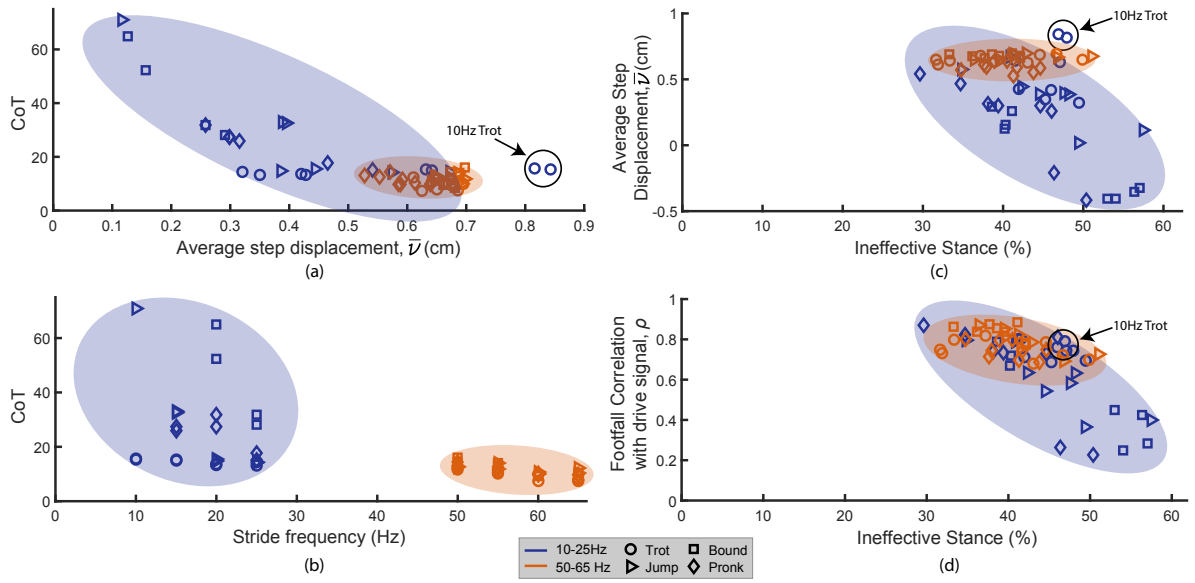

Figure 8: (a) Cost of transport vs. average step displacement (b) Cost of transport vs. stride frequency (c) Average step displacement vs. ineffective stance. (d) Correlation of footfall z-position in world frame with drive signal vs. ineffective stance.

Table 2: Input conditions and calculated metrics for six HAMR gaits

Input Conditions			**Performance Metrics**			
Gait	Stride Frequency (Hz)	Energy ($^{mJ}/_{stride}$)	Speed ($BL\,s^{-1}$)	Normalized Speed ($^{mm}/_{stride}$)	Ineffective stance ($\bar{I}_s$, %)	CoT
Trot	10	1.80	1.8	8.2	48	14
Trot	15	1.35	2.1	6.4	42	15
Trot	65	0.72	9.9	6.8	44	7.5
Pronk	55	0.97	6.7	5.5	44	12
Jump	60	0.97	8.5	6.4	40	10
Bound	60	0.88	8.8	6.6	38	9.3

ing ineffective stance and thereby resulting in a further reduction of input energy. Preliminary results for CoT are described in the following paragraphs, however a more detailed study on design and control of stiffness and damping properties for increased efficiency is left for future work.

Figure 8a shows the CoT as a function of average step displacement for all gaits. The minimum CoT for HAMR is 7.4 during the 60 Hz trot, compared to 15.7 for the 10 Hz trot. The mean CoT for gaits in the low frequency regime is 23.5 ± 13.2 (n=25) compared to 11.1 ± 2.1 (n=32) in the high frequency regime[i]. The CoT is lower on average in the high frequency regime compared to the low frequency regime. Comparing the CoT for the two frequency regimes, we find that there is a significant difference [ANOVA, $P = 0.03, F_{(3,42)} = 3.3$; Fig. 8a,b].

3.4 Main challenges: ground contact affecting footfall correlation and slipping

Body dynamics affect ground contact and these variations can impact the levels of ineffective stance and correlation with the prescribed footfall patterns. These metrics are discussed in the following subsections.

3.4.1 Ineffective Stance

Ineffective stance ($\bar{I}_s$) is shown in Fig. 8c, d and Table 2 and is above 25% for all tested gaits, which is largely attributed to the smooth cardstock running surface. Ineffective stance is more variable in the low frequency regime ($45 \pm 7\%$, n=32) compared to the high frequency regime ($40 \pm 5\%$, n=32), however this difference is not significant [ANOVA, $P = 0.11, F_{(3,42)} = 2.1$; Fig. 8c, d]. In the low frequency regime, ineffective stance and average step displacement are inversely correlated. In the high frequency regime, however, they seem to be uncorrelated. One explanation for this is that the amplitude of body oscillations are attenuated in the high frequency regime which reduces the likelihood that the footfall pattern deviates from the open-loop command.

3.4.2 Footfall Correlation

Footfall patterns of the high frequency gaits follow the commanded gait phasing more closely than the low frequency gaits as shown in Fig. 8d. This differentiates HAMR locomotion from other vibratory

[i]Only trials with forward locomotion are considered for CoT analysis – seven trials in the low frequency regime moved backwards.

modes (low gait correlation) of locomotion. The correlation of the footfall with the actuator signals is (0.86 ± 0.03, n=32) in the high frequency regime compared to (0.72 ± 0.17, n=32) in the low frequency regime. Figure 8d shows that as footfall deviates from the commanded drive signal (i.e. lower footfall correlation with drive signal, ρ), the legs experience higher levels of ineffective stance. This indicates that the ineffective stance metric is informative of how well the foot contact follows the commanded footfall pattern. Furthermore, there is a significant difference between the correlation with the drive signal in the two frequency regimes [ANOVA, $P = 0.04, F_{(3,42)} = 3.0$; Fig. 8d]. Two remedies to high ineffective stance and lower correlation with the drive signals in the body dynamics regime could be changes in the foot design or feedback control to realize optimized footfall patterns using ground contact sensing.

3.5 Cross-platform comparison

In order to put the analysis of HAMR in context, Table 3 summarizes HAMR's performance relative to three other similarly sized legged systems. Speed, ineffective stance, and CoT are calculated using kinematic data from three other legged systems: the "flying monkey" (Koh et al., 2016), the commercial version of DASH (Birkmeyer et al., 2009), and the *Blaberus discoidalis* cockroach.

The flying monkey and DASH robots have relatively higher levels of ineffective stance compared to HAMR. Speeds of 9.2 and 6.5 $\mathrm{BL\,s^{-1}}$ are achieved for the flying monkey and DASH which suggests that higher speeds would be possible with improvements to the gaits and running surfaces.

Table 3: Cross-platform comparison for Speed, Ineffective Stance, and CoT.

	Normalized Performance Metrics			
Platform*	Stride Frequency (Hz)	Normalized Speed ($^{\mathrm{BL}}/_{\mathrm{stride}}$)	Ineffective stance ($\bar{\mathrm{I}}_{\mathrm{s}}$, %)	CoT
HAMR-VI‡	1-25	0.05	45	24
HAMR-VI‡	50-65	0.14	40	11
Flying Monkey	52	0.18	56	12
DASH	18.7	0.35	60	1.5
Blaberus discoidalis	14.9	0.93	5	6.0§

*Specifications: HAMR-VI (45.1mm, $1.43\,\mathrm{g}$), Flying Monkey ($40.0\,\mathrm{mm}$, $8.6\,\mathrm{g}$), DASH ($118\,\mathrm{mm}$, $16\,\mathrm{g}$), *Blaberus discoidalis* ($41.7\,\mathrm{mm}$, $4.1\,\mathrm{g}$).

‡ Reported values are the mean of the 32 trials in each regime.

§ The CoT for *Blaberus discoidalis* is computed from (Herreid and Full, 1984) with a conversion of $1\,\mathrm{L}$ of $\mathrm{O_2} = 20.7\,\mathrm{kJ}$ from (Mann and Truswell, 2012).

Blaberus discoidalis is the fastest of the legged systems considered here relative to body size at $13.8\,\mathrm{BL\,s^{-1}}$ and has the lowest ineffective stance of 5%. This suggests that the ineffective stance metric is capturing foot slippage appropriately since it is known from the biological experiments that *Blaberus discoidalis* has little foot slippage even during the presence of perturbations (Jindrich and Full, 2002).

The minimum CoT of HAMR (7.4) is similar to other systems at the same length scale. For example, *Blaberus discoidalis* has a CoT of 6. DASH and the "Flying Monkey" have a CoT of 1.5 and 12, respectively. However, cost of transport is know to scale with mass, where larger systems typically have a lower CoT (Kram and Taylor, 1990). It is also important to mention that the results in this paper are for a tethered version of HAMR, whereas the other systems in Table 3 are power autonomous. Despite the advantage of having offboard power, a power autonomous version of HAMR (HAMR-F, (Goldberg

et al., 2017c)) maintains eight independently actuated DOFs and shows remarkably similar speeds up to stride frequencies of $35\,\mathrm{Hz}$ (due to microcontroller limitations, the stride frequency is limited to $35\,\mathrm{Hz}$), with a top speed of $3.8\,\mathrm{BL\,s^{-1}}$ and a CoT of 85. The main difference in the power autonomous version is in overall mass and power consumption. There is an overhead for high voltage generation that results in a power consumption that is an order of magnitude higher than the tethered version of the robot ($480\,\mathrm{mW}$ vs. $48\,\mathrm{mW}$ at $15\,\mathrm{Hz}$). The high power consumption is primarily due to the overhead in high voltage and control signal generation. The mass of HAMR-F, including a battery, is $2.79\,\mathrm{g}$ compared to $1.43\,\mathrm{g}$ for HAMR-VI.

4 Conclusion

In this paper, we apply locomotion metrics relevant to small scale locomotion and analyze a large quantity of gaits on HAMR. We analyzed 32 distinct operating conditions spanning stride frequencies from 10-65Hz. More importantly, these frequencies cover two important regimes: one where the stride frequency is near the body natural frequencies, and one where the stride frequency is more than double the average of the body natural frequencies.

In the low frequency regime, we find that speed and footfall correlation is highly variable. Despite these variations, some high performing gaits have energy characteristics similar to SLIP-like running (e.g. the 10 and 15Hz Trots). This suggests that it is possible to fine-tune and control other gaits that suffer from destructive body dynamics in this regime. However, without proprioceptive sensing and feedback control (a challenge at the insect-scale), it is difficult to tune these gaits around body modes for a given body morphology. Additionally, manufacturing and material variations can lead to unpredictable dynamics, making it difficult to stabilize the body dynamics to specific limit-cycles.

In contrast, the open-loop dynamics in the high frequency regime consistently result in high performing gaits. We hypothesize that the simplified lateral and angular control scheme presented in (Goldberg et al., 2017b) is possible due to the reduced impact of body dynamics in the high frequency regime. Additionally, we hypothesize that there will be a greater advantage for CoT in the high frequency regime due to the smaller relative contribution of the overhead cost of onboard, high voltage generation as measured in Goldberg et al.

Stride frequency and body dynamics are typically constraints for legged runners due to bandwidth limitations of actuators. In these cases, gait changes such as leg phasing and stride length can be leveraged to increase speed. In contrast, this paper shows that we are able to utilize the high bandwidth piezoelectric actuators in HAMR to operate in a frequency regime that surpasses the resonant body modes of the robot. In terms of performance, we see that when operating in this regime, different gaits tend to have similar speeds and exhibit kinematic running energy profiles. Furthermore, the footfall patterns of the gaits remain highly correlated with the centralized, feedforward control signals. In other words, footfalls are not stochastic as utilized by some vibration-based, "legged" robots – e.g., HEXBUG and kilobot (Rubenstein et al., 2012).

The trend we report in this paper towards kinematic running at high stride frequencies is consistent with scaling trends into the micro scale domain – inertial forces become less significant with a decrease in scale, suggesting a shift from dynamic motion to kinematic motion. As we observe in the high frequency regime, control strategies for this type of locomotion will likely be different: one hypothesis is that position control (i.e. proprioceptive leg position) will be more important than force control (i.e. controlling SLIP force profiles). A robotic platform such as HAMR can help bridge the gap and explore different running strategies at millimeter scales. Overall, this analysis shows that HAMR is a multipurpose legged microrobotic platform with the potential for a wide range of applications, including testing biological hypotheses in neuromechanics, locomotion, and control. Furthermore, the tools, metrics, and

methods outlined here are independent of size and can be used across platforms for studying gait in legged locomotion.

5 Future Work

The experimental analysis presented here is a new methodology for studying gait selection in a legged robot with complex dynamics. Hypotheses regarding relative stiffness and body dynamics are easy to test on HAMR. For example, based on the results here, one hypothesis is that a higher leg stiffness might be beneficial given the high force/high bandwidth piezoelectric actuators. Changes to the relative stiffness can alter the frequency where SLIP locomotion naturally occurs (i.e. without force control). This could optimize speed and efficiency for a range of applications – for example inspection tasks in confined spaces or search and rescue for natural disasters or surveillance.

Beyond running straight on flat terrain, this methodology and the new metrics will be applied to other locomotion scenarios such as experiments on perturbation rejection, maneuverability, leg trajectory control, climbing, and locomotion on different surfaces. For example, more stable gaits could result in higher relative performance on uneven terrain, and lower levels of ineffective stance could improve climbing capabilities. Such correlations could identify these metrics as valid objectives for designing gaits to accomplish a variety of tasks. The gait analysis can also elucidate the amount of centralization or sensory feedback needed for future applications requiring high speed and efficient running.

Acknowledgments

The authors thank all members of the Microrobotics Lab for valuable discussions. In particular, we thank Prof. Ardian Jusufi, Prof. Onur Ozcan and Prof. Nick Gravish for helpful discussions on characterizing the locomotion of HAMR. Thanks to Prof. Todd Zickler for help developing the locomotion reconstruction analysis during a class project in his Computer Vision class.

Funding

This work is partially funded by the Wyss Institute for Biologically Inspired Engineering and the National Science Foundation. This material is based upon work supported by the National Science Foundation Graduate Research Fellowship under Grant Number DGE1144152. Any opinion, findings, and conclusions or recommendations expressed in this material are those of the authors and do not necessarily reflect the views of the National Science Foundation. In addition, the prototypes were enabled by equipment supported by the ARO DURIP program (award #W911NF-13-1-0311)

References

Bailey, S. A., Cham, J. G., Cutkosky, M. R., and Full, R. J. (2001). Comparing the locomotion dynamics of the cockroach and a shape deposition manufactured biomimetic hexapod. In *Experimental Robotics VII*, pages 239–248. Springer.

Baisch, A. T. (2013). *Design, Manufacturing, and Locomotion Studies of Ambulatory Micro-Robots*. PhD thesis, Harvard University School of Engineering and Applied Sciences.

Baisch, A. T., Ozcan, O., Goldberg, B., Ithier, D., and Wood, R. J. (2014). High speed locomotion for a quadrupedal microrobot. *The International Journal of Robotics Research*, 33(8):1063–1082.

Baisch, A. T. and Wood, R. J. (2011). Design and Fabrication of the Harvard Ambulatory Micro-Robot. In *Robotics Research*, pages 715–730. Springer.

Birkmeyer, P., Gillies, A. G., and Fearing, R. S. (2012). Dynamic climbing of near-vertical smooth surfaces. In *IEEE/RSJ Intl. Conf. on Intelligent Robots and Systems*, Vilamoura, Portugal.

Birkmeyer, P., Peterson, K., and Fearing, R. S. (2009). DASH: A dynamic 16g hexapedal robot. In *IEEE/RSJ Intl. Conf. on Intelligent Robots and Systems*, pages 2683–2689. IEEE.

Blickhan, R. and Full, R. (1993). Similarity in multilegged locomotion: bouncing like a monopode. *Journal of Comparative Physiology A*, 173(5):509–517.

Bruhwiler, R., Goldberg, B., Doshi, N., Ozcan, O., Jafferis, N., Karpelson, M., and Wood, R. J. (2015). Feedback control of a legged microrobot with on-board sensing. In *Intelligent Robots and Systems (IROS), 2015 IEEE/RSJ International Conference on*, pages 5727–5733. IEEE.

Cavagna, G. A., Heglund, N. C., and Taylor, C. R. (1977). Mechanical work in terrestrial locomotion: two basic mechanisms for minimizing energy expenditure. *American Journal of Physiology-Regulatory, Integrative and Comparative Physiology*, 233(5):R243–R261.

Chen, J., Peattie, A., Autumn, K., and Full, R. (2006). Differential leg function in a sprawled-posture quadrupedal trotter. *Journal of Experimental Biology*, 209(2):249–259.

Doshi, N., Goldberg, B., Sahai, R., Jafferis, N., Aukes, D., and Wood, R. J. (2015). Model driven design for flexure-based microrobots. In *Intelligent Robots and Systems (IROS), 2015 IEEE/RSJ International Conference on*, pages 4119–4126. IEEE.

Doshi, N., Jayaram, K., Goldberg, B., and Wood, R. J. (2017). Phase control for a legged microrobot operating at resonance. *2017 IEEE International Conference on Robotics and Automation (ICRA)*.

Full, R., Blickhan, R., and Ting, L. (1991). Leg design in hexapedal runners. *Journal of Experimental Biology*, 158(1):369–390.

Full, R. J. and Koditschek, D. E. (1999). Templates and anchors: neuromechanical hypotheses of legged locomotion on land. *Journal of Experimental Biology*, 202(23):3325–3332.

Full, R. J., Kubow, T., Schmitt, J., Holmes, P., and Koditschek, D. (2002). Quantifying dynamic stability and maneuverability in legged locomotion. *Integrative and comparative biology*, 42(1):149–157.

Full, R. J. and Tu, M. S. (1991). Mechanics of a rapid running insect: two-, four-and six-legged locomotion. *Journal of Experimental Biology*, 156(1):215–231.

Goldberg, B., Doshi, N., and Wood, R. J. (2017a). A high speed motion capture method and performance metrics for studying gaits on an insect-scale legged robot. *Under Review: 2017 IEEE International Conference on Robotics and Automation (ICRA)*.

Goldberg, B., Doshi, N., and Wood, R. J. (2017b). High speed trajectory control using an experimental maneuverability model for an insect-scale legged robot. *2017 IEEE International Conference on Robotics and Automation (ICRA)*.

Goldberg, B., Zufferey, R., Whittredge, G., Doshi, N., Helbling, F. E., Kovac, M., and Wood, R. J. (2017c). Wireless control and power autonomy for a high-speed legged microrobot. *Under Review: IEEE/RSJ International Conference on Intelligent Robots and Systems 2017*.

Haldane, D. W., Casarez, C. S., Karras, J. T., Lee, J., Li, C., Pullin, A. O., Schaler, E. W., Yun, D., Ota, H., and Javey, A. (2015). Integrated manufacture of exoskeletons and sensing structures for folded millirobots. *Journal of Mechanisms and Robotics*, 7(2):021011.

Haldane, D. W. and Fearing, R. S. (2015). Running beyond the bio-inspired regime. In *2015 IEEE International Conference on Robotics and Automation (ICRA)*, pages 4539–4546. IEEE.

Haldane, D. W., Peterson, K. C., Bermudez, F. L. G., and Fearing, R. S. (2013). Animal-inspired design and aerodynamic stabilization of a hexapedal millirobot. In *2013 IEEE International Conference on Robotics and Automation (ICRA)*, pages 3279–3286. IEEE.

Heglund, N. C., Cavagna, G. A., and Taylor, C. R. (1982). Energetics and mechanics of terrestrial locomotion. iii. energy changes of the centre of mass as a function of speed and body size in birds and mammals. *Journal of Experimental Biology*, 97(1):41–56.

Herreid, C. F. and Full, R. J. (1984). Cockroaches on a treadmill: aerobic running. *Journal of insect physiology*, 30(5):395–403.

Holmes, P., Full, R. J., Koditschek, D., and Guckenheimer, J. (2006). The dynamics of legged locomotion: Models, analyses, and challenges. *Siam Review*, 48(2):207–304.

Hoover, A. M., Steltz, E., and Fearing, R. S. (2008). RoACH: An autonomous 2.4g crawling hexapod robot. In *IEEE/RSJ Intl. Conf. on Intelligent Robots and Systems*, pages 22–26.

Jafferis, N. T., Graule, M. A., and Wood, R. J. (2016a). Non-linear resonance modeling and system design improvements for underactuated flapping-wing vehicles. In *2016 IEEE International Conference on Robotics and Automation (ICRA)*, pages 3234–3241. IEEE.

Jafferis, N. T., Lok, M., Winey, N., Wei, G.-Y., and Wood, R. J. (2016b). Multilayer laminated piezoelectric bending actuators: design and manufacturing for optimum power density and efficiency. *Smart Materials and Structures*, 25(5):055033.

Jayaram, K. and Full, R. J. (2016). Cockroaches traverse crevices, crawl rapidly in confined spaces, and inspire a soft, legged robot. *Proceedings of the National Academy of Sciences*, 113(8):E950–E957.

Jindrich, D. L. and Full, R. J. (2002). Dynamic stabilization of rapid hexapedal locomotion. *Journal of Experimental Biology*, 205(18):2803–2823.

Jusufi, A., Goldman, D. I., Revzen, S., and Full, R. J. (2008). Active tails enhance arboreal acrobatics in geckos. *Proceedings of the National Academy of Sciences*, 105(11):4215–4219.

Koh, J.-S., Aukes, D. M., Araki, B., Pohorecky, S., Mulgaonkar, Y., Tolley, M. T., Kumar, V., Rus, D., and Wood, R. J. (2016). A modular folded laminate robot capable of multi modal locomotion. In *International Symposium on Experimental Robotics (ISER 2016), Tokyo, Japan, Oct., 2016*.

Kram, R. and Taylor, C. R. (1990). Energetics of running: a new perspective. *Nature*, 346(6281):265.

Mann, J. and Truswell, S. (2012). *Essentials of human nutrition*. Oxford University Press.

Mazouchova, N., Gravish, N., Savu, A., and Goldman, D. I. (2010). Utilization of granular solidification during terrestrial locomotion of hatchling sea turtles. *Biology letters*, 6(3):398–401.

Mazouchova, N., Umbanhowar, P. B., and Goldman, D. I. (2013). Flipper-driven terrestrial locomotion of a sea turtle-inspired robot. *Bioinspiration & biomimetics*, 8(2):026007.

Noh, M., Kim, S.-W., An, S., Koh, J.-S., and Cho, K.-J. (2012). Flea-inspired catapult mechanism for miniature jumping robots. *Robotics, IEEE Transactions on*, 28(5):1007–1018.

Reinhardt, L., Weihmann, T., and Blickhan, R. (2009). Dynamics and kinematics of ant locomotion: do wood ants climb on level surfaces? *The Journal of experimental biology*, 212(15):2426–2435.

Roberts, S. F. and Koditschek, D. E. (2016). RHex slips on granular media. In *IEEE International Conference on Robotics and Automation*.

Rubenstein, M., Ahler, C., and Nagpal, R. (2012). Kilobot: A low cost scalable robot system for collective behaviors. In *2012 IEEE International Conference on Robotics and Automation (ICRA)*, pages 3293–3298. IEEE.

Rubin, S., Young, M. H.-Y., Wright, J. C., Whitaker, D. L., and Ahn, A. N. (2016). Exceptional running and turning performance in a mite. *Journal of Experimental Biology*, 219(5):676–685.

Seitz, B. F., Goldberg, B., Doshi, N., Ozcan, O., Christensen, D. L., Hawkes, E. W., Cutkosky, M. R., and Wood, R. J. (2014). Bio-inspired mechanisms for inclined locomotion in a legged insect-scale robot. In *Robotics and Biomimetics (ROBIO), 2014 IEEE International Conference on*, pages 791–796. IEEE.

Sreetharan, P. S., Whitney, J. P., Strauss, M. D., and Wood, R. J. (2012). Monolithic fabrication of millimeter-scale machines. *Journal of Micromechanics and Microengineering*, 22(5):055027.

St Pierre, R. and Bergbreiter, S. (2016). Gait exploration of sub-2 g robots using magnetic actuation. *IEEE Robotics and Automation*.

Strogatz, S. H. (2014). *Nonlinear dynamics and chaos: with applications to physics, biology, chemistry, and engineering*. Westview press.

Ting, L., Blickhan, R., and Full, R. (1994). Dynamic and static stability in hexapedal runners. *Journal of Experimental Biology*, 197(1):251–269.

Vogtmann, D., Pierre, R. S., and Bergbreiter, S. (2017). A 25 mg magnetically actuated microrobot walking at$>$ 5 body lengths/sec. In *Micro Electro Mechanical Systems (MEMS), 2017 IEEE 30th International Conference on*, pages 179–182. IEEE.

Supplementary Material

S1 Video: Example tracking of 30 Hz jump gait

S2 Video: Six different gaits at 60 Hz stride frequency

S3 Video: Progression of the pronk gait with increasing stride frequency

S4 Video: Highly dynamic gaits

S5 Input electrical power

Jafferis et al. has shown that an estimate of the power for a single optimal energy density, piezoelectric bimorph actuator approximately follows the power consumption of a capacitor (Jafferis et al., 2016b):

$$\overline{P}_{in} = \frac{1}{2}\frac{\epsilon_o A}{t} V_{\text{bias}}^2 f \tag{3}$$

Where ϵ_o is the dielectric constant, A is the area of the actuator, t is the thickness of the piezoelectric material, V_{bias} is the peak-to-peak actuation voltage, and f is the actuation frequency. Assuming the dielectric constant and capacitance of the actuator does not change substantially with voltage or frequency, this becomes:

$$\overline{P}_{in} \approx \text{k}_\text{P} V_{\text{bias}}^2 f \tag{4}$$

Where k_P is an experimentally-measured power constant. This constant allows us to estimate input electrical power given a drive voltage, V_{bias}, and stride frequency, f. The experimental power constant is measured to be $8 \times 10^{-8}\text{J/V}^{-2}$.

A power autonomous robot, however, will have a higher k_P than this due to losses in the power electronics and other inefficiencies of onboard control. Considerations for the effects of power consumption of a power autonomous robot are made in Sec. 3.5.

S6 Amplitude-normalized Stride Correlation (ANSC)

ANSC Definition In addition to speed and efficiency, stability is also important to consider. To this end, there are formal definitions of stability for hybrid dynamic running systems; for example, using Floquet analysis Strogatz (2014). Other approaches for small scale runners look at static and dynamic stability Ting et al. (1994); Full et al. (2002) or experimental metrics that compare the deviations in energy from stride to stride Haldane et al. (2013). The proposed metric of ANSC is a measure of the amplitude and periodicity of body dynamics that can be used to inform a sense of stability. The strength of this analysis is that it does not require a detailed model and it is dimensionless, allowing for comparisons across length scales.

For level-ground running, we propose ANSC as a quantitative measure of the smoothness and repeatability of a gait. This metric is similar to the measure of stable energy limit cycles in Haldane et al., but takes into consideration both the periodicity and amplitude of the body modes and is normalized by characteristic length (where appropriate) to allow for a dimensionless, cross-platform comparison. The definition of this metric is described in detail in (Goldberg et al., 2017a) and a brief summary is given here:

If in a limit cycle, the body modes (i.e., x-y-z-roll-pitch-yaw) are expected to be periodic at the prescribed stride frequency or dominant observed frequency. As such, the time course data is segmented into a collection of cycles with period equal to the inverse of the dominant frequency. A qualitative example of this segmentation for the body oscillations is shown in Fig. 9.

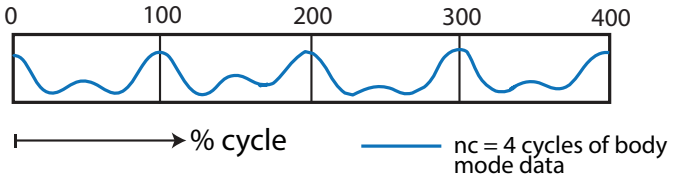

Figure 9: Example of segmenting body oscillation data for use in calculating amplitude-normalized stride correlation.

The ANSC of a body mode for a given cycle size is computed by taking the average correlation coefficient between cycles, r_m. Values range from -1 to 1, with a values close to 1 implying limit cycle behavior at the considered frequency. The ANSC of a body mode, s_m, is defined as r_m divided by the root-mean-square (RMS_m) magnitude of oscillation for that body mode. For body position modes, the quantity is normalized by the body length (L): $s_m^{xyz} = {}^{(r_m L)}/_{\text{RMS}_m}$ and for body angles, ANSC is: $s_m^{\theta\phi\psi} = {}^{(r_m)}/_{\text{RMS}_m}$.

As defined above, ANSC is dimensionless and while the lower bound of ANSC is zero, there is no upper bound as RMS oscillations can be arbitrarily small. However, relative comparisons can still be made; for example, a two-fold increase in ANSC can be due to either of the following (or some partial combination): doubling the cyclical correlation, doubling the length scale (i.e., a larger body), or halving the magnitude of RMS body oscillations. Baseline measures of ANSC in Fig. 10 and Table 4 give an idea of typical ranges for ANSC. In order to account for the complete sagittal plane, the ANSC presented in this paper is an average of the forward (x), vertical (z), and pitch (ϕ) DOFs. Furthermore, this metric can be applied to systems beyond those explored in this paper (the Flying Monkey, DASH, and *Blaberus discoidalis*) where periodicity arises autonomously and is not explicitly enforced by using a discrete Fourier transform to determine the frequency of the limit cycle (the dominant observed frequency).

ANSC for HAMR-VI and other legged systems The ANSC for HAMR (average of x, z and *pitch* modes) is higher in the high frequency regime (77.8 ± 41.5, n=32) compared to the low frequency regime

(56.2 ± 39.9, n=32). Comparing the two regimes, there is a significant difference in ANSC [ANOVA, $P = 0.003, F_{(3,42)} = 4.9$; Fig. 10]. While high ANSC is typically observed with high average step displacements (Fig. 10), instabilities in HAMR may eventually be exploited and controlled for highly dynamic and high performance gaits. For comparison, the ANSC for three other legged systems is shown in Table 4. This highest observed stability is for *Blaberus discoidalis*, with an ANSC of 94.

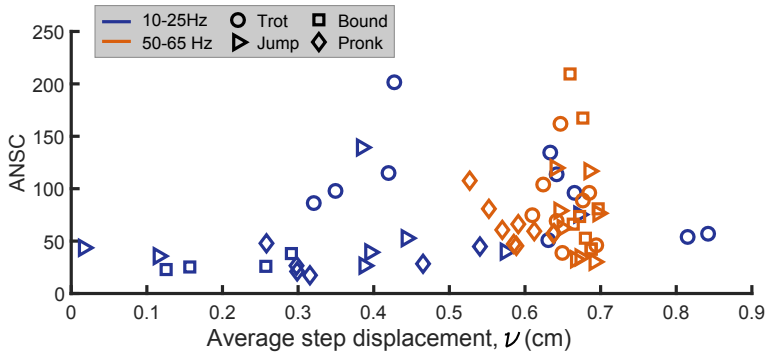

Figure 10: ANSC for HAMR vs. average step displacement in the high and low stride frequency regimes.

Table 4: Cross-platform comparison ANSC.

	Normalized Performance Metrics		
Platform*	Stride Frequency (Hz)	Speed ($^{BL}/_{s}$)	ANSC
HAMR-VI‡	1-25	1	56
HAMR-VI‡	50-65	8.3	77
Flying Monkey	52	9.2	21
DASH	18.7	6.5	11
Blaberus discoidalis	14.9	13.8	94

‡ Reported values are the mean of the 32 trials in each regime .
§ The CoT for *Blaberus discoidalis* is computed from (Herreid and Full, 1984) . with a conversion of 1 L of $O_2 = 20.7$ kJ from (Mann and Truswell, 2012)

S7 Data: MATLAB structure of the complete dataset

The attached MATLAB structure contains data for all of the HAMR trials conducted in this study.